Soft Matter

PAPER

Rheology of reconstituted silk fibroin protein gels: the epitome of extreme mechanics

A. Pasha Tabatabai,[a] David L. Kaplan[b] and Daniel L. Blair*[a]

Cite this: *Soft Matter*, 2015, **11**, 756

Received 16th September 2014
Accepted 1st December 2014

DOI: 10.1039/c4sm02079k

www.rsc.org/softmatter

In nature, silk fibroin proteins assemble into hierarchical structures with dramatic mechanical properties. With the hope of creating new classes of on demand silk-based biomaterials, *Bombyx mori* silk is reconstituted back into stable aqueous solutions that can be reassembled into functionalized materials; one strategy for reassembly is electrogelation. Electrogels (e-gels) are particularly versatile and can be produced using electrolysis with small DC electric fields. We characterize the linear and nonlinear rheological behavior of e-gels to provide fundamental insights into these distinct protein-based materials. We observe that e-gels form robust biopolymer networks that exhibit distinctive strain hardening and are recoverable from strains as large as $\gamma = 27$, *i.e.* 2700%. We propose a simple microscopic model that is consistent with local restructuring of single proteins within the e-gel network.

1 Introduction

The use of silk for the production of materials spans more than two millennia.[1] Recently, the interest in extending the commercial uses of silk to new biomedical applications is driving the development of new technologies capable of producing on-demand therapeutic materials. In many instances, the feedstock for new silk based biomaterials are the hydrophobic spun threads produced by *Bombyx mori* silk worms.[1–5]

Reconstituting silk avoids harvesting silk from a live animal by starting the process with pre-spun cocoons.[6–8] These cocoons are reconstituted into an aqueous silk protein solution similar to native silk and transformed into functionally specific forms for use in biomedicine such as gels, films, and sponges.[1,3–5] A novel fibroin protein design of biomedical interest utilizes electrochemistry to convert the fibroin solution into a gel (e-gel). The e-gel is versatile in the biomedical world because it is tunably adhesive, reversible, high strength, and resilient to shear.[2,3,9] These attributes, combined with silk's biodegradability, can be utilized for *in situ* gelation, providing a functional matrix for use in tissue engineering.[10]

Characterizing the linear and nonlinear rheology of reconstituted silk gels is an essential step toward understanding how they can be more efficiently processed into programmable materials. Previous work has measured the e-gel rheology in the linear regime, although the presence of bubbles likely affects the measured rheological properties.[2,3] Consequently, we have developed a technique to remove unwanted bubbles from the e-gel providing a more robust initial state for rheological measurements. The e-gel's use as a biomaterial creates scenarios where it will be far from mechanical equilibrium, a regime that is currently unexplored. In this work, we present linear and nonlinear rheology of the e-gel to create a complete picture for the e-gel viscoelasticity. We observe that the e-gel has rheological properties that are remarkably different from other *in vitro* biopolymer systems including an extraordinarily large yield strain and a strain hardening response. Additionally, we show that deviations from expected polymer rheology can be described through a simple picture that incorporates shear history through inter-protein binding.

2 Method

2.1 Reconstitution

Bombyx mori cocoons are primarily composed of two proteins: sericin and fibroin. Because sericin produces adverse reactions *in vivo*, it is removed by boiling the cocoons for 10 minutes in aqueous 0.02 M sodium carbonate. The resulting hydrophobic fibroin protein threads are rinsed and dried overnight. The fibroin is solubilized by soaking in aqueous 9.3 M lithium bromide at 60 °C for 2 hours, then dialyzed against cycled deionized water for 48 hours.[11] The final reconstituted aqueous silk fibroin solution is approximately 5% (w/w).

2.2 Electrogelation

E-gels are made by placing a 125 μL droplet of protein solution within a parallel plate capacitor comprised of a platinum sputtered glass plate and an aluminum plate separated by 0.5 mm. A DC electric potential of 5 V is placed across the capacitor for 15 minutes; the platinum electrode is the cathode. A gel begins to form on the cathode and grows towards the anode,

[a]*Georgetown University, Department of Physics, The Institute for Soft Matter Synthesis and Metrology, Washington, DC 20057, USA. E-mail: Daniel.Blair@georgetown.edu*
[b]*Tufts University, Department of Biomedical Engineering, Medford, MA 02155, USA*

reaching steady state when it spans approximately 60% of the gap. E-gel formation is a result of local pH changes due to electrodiffusion of H^+ and OH^- ions created during the hydrolysis of water.[12] We remove the anode and wick away the ungelled solution from the e-gel surface to avoid any recombination between basic and acidic regions.

Hydrogen bubbles created during the hydrolysis procedure are removed from the e-gel prior to all rheological measurements. Care is taken to avoid deformations that may lead to structural changes within the e-gel at each step of the processing since large shear stresses and dehydration can induce irreversible mechanical changes.[11] To eliminate bubbles, we centrifuge the e-gel that is pinned by surface tension as a sessile drop on the platinum electrode at an acceleration of 500 g for 5 minutes, we then place the e-gel in a rapid vacuum desiccator to eliminate any residual bubbles at the surface. To compensate for any water loss, we dip the e-gel in room temperature DI water (pH 6); this is sufficient to rehydrate the e-gel without any additional swelling.

2.3 Rheology

To perform rheological measurements, we affix the gel-electrode system to the rheometer base and lower the measuring tool at a rate of 5 μm s^{-1} to minimize the magnitude of the radial shear stress imparted onto the e-gel. All rheological measurements are performed using an Anton Paar MCR-301 stress controlled rheometer using a 25 mm cone-plate tool with a cone angle of 1.001° and a truncation height of 49 μ;m. A cone-plate geometry is chosen to avoid the entrapment of air between the irregular surface of the e-gel and the rheometer tool that is unavoidable with a parallel-plate tool.

3 Silk fibroin: structure and assembly

The 350 kDa amino acid sequence contains 12 long repetitive glycine–alanine rich domains separated by shorter amorphous linkers.[13] These long domains are known to form β-sheets in the fiber form and are commonly referred to as the crystalline regions.[6,13–15] However, the reconstitution process is designed to break apart hydrogen bonded structures like β-sheets. In reconstituted solutions, the fibroin protein is predominantly unstructured, and when transformed into an e-gel, measurements have seen both random and α-helical content.[3,9,11]

During electrogelation the fibroin in solution is thought to assemble into micelles that further collect into aggregates.[3,9,16] These structures deform under shear, exposing inter-micelle hydrophobic groups thus creating fibrils. It is likely that the difference between the secondary structure in the e-gel and in the silk fiber is correlated with the fibroin hierarchical assembly; the e-gel may need an input of shear energy for the micelles to coalesce and form β-sheets.

4 Results

We first quantify the flow properties of the ungelled silk solution with a shear rate ramp from $\dot{\gamma} = \frac{d\gamma}{dt} = 10^{-2}$ to 10^{2} s^{-1} while measuring the steady-state stress response, which we found to be reversible [Fig. 1]. The resulting flow curve is fit to a Herschel–Bulkley relation

$$\sigma(\dot{\gamma}) = \sigma_y + K\dot{\gamma}^{\beta}, \quad (1)$$

with a yield stress $\sigma_y = 0.2$ Pa and $\beta = 1$, indicating that the solution has the hallmarks of a Bingham plastic with liquid-like characteristics above the yield stress. The yield stress may originate from protein interactions in the bulk or through adsorption of the protein at the air–water interface.[17]

The difference in mechanical properties of the silk before and after the electrogelation process are dramatic. We measure the storage G' and loss G'' moduli of both the solution and e-gel using oscillatory rheology; the strain amplitude is varied from $\gamma = 10^{-3}$ to 10^{0} at a fixed frequency $f = 0.5$ Hz [Fig. 2(a)]. The solution exhibits the signatures of a weak viscoelastic fluid – predominantly fluid-like behavior over the entire range of γ – consistent with the flow curve in Fig. 1. However, the modulus of the e-gel is more than three orders of magnitude greater than that of the solution. Additionally, the e-gel has a corresponding loss tangent $\tan(\delta) \sim 0.1$ indicative of an elastic solid. Over a broad range of frequencies at a fixed $\gamma = 10^{-2}$, the e-gel moduli exhibit a weak power law increase, reminiscent of a glassy or gel-like response observed for a broad class of materials [Fig. 2(b)].[18,19] At low frequencies, the moduli of the solution are roughly equivalent but exhibit a slight frequency dependence. This linear rheology is qualitatively similar to previous measurements.[2,3]

The mesh size for a gel composed of flexible polymers is estimated as $\xi \sim (k_b T/G)^{1/3}$, where k_b is Boltzmann's constant and T is the absolute temperature. Using the measured linear shear modulus, this relation predicts $\xi \sim 100$ nm, much larger than the measured Kuhn length, suggesting that we may consider the linear response of silk fibroin e-gels as consistent with that of flexible polymers.[20]

We utilize a stress relaxation test to probe the large deformation behavior of the e-gel. A stepwise increasing rotational

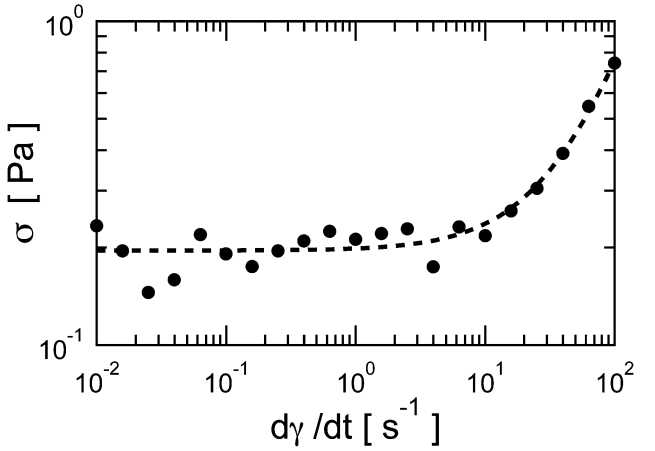

Fig. 1 The rheological results of a shear rate ramp (●) of one ungelled reconstituted silk fibroin solution at a concentration of 5% (w/w). The shear stress is fit to a Herschel–Bulkley relation (dashed line) with a small stress plateau and an exponent of 1.

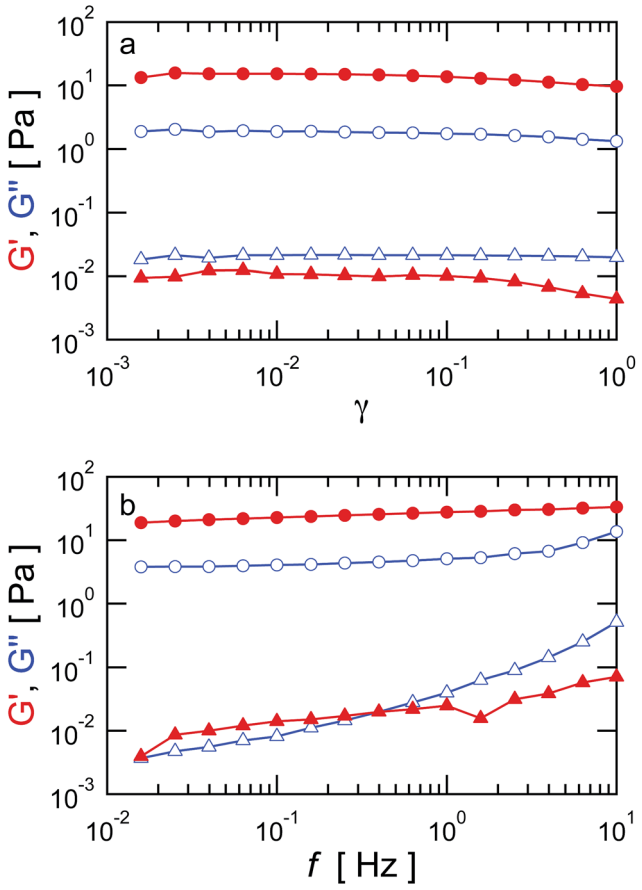

Fig. 2 G' (closed symbols) and G'' (open symbols) of one silk fibroin solution (△) and one e-gel (○) through a linear viscoelastic (a) strain sweep at $f = 0.5$ Hz and (b) frequency sweep at $\gamma = 10^{-2}$.

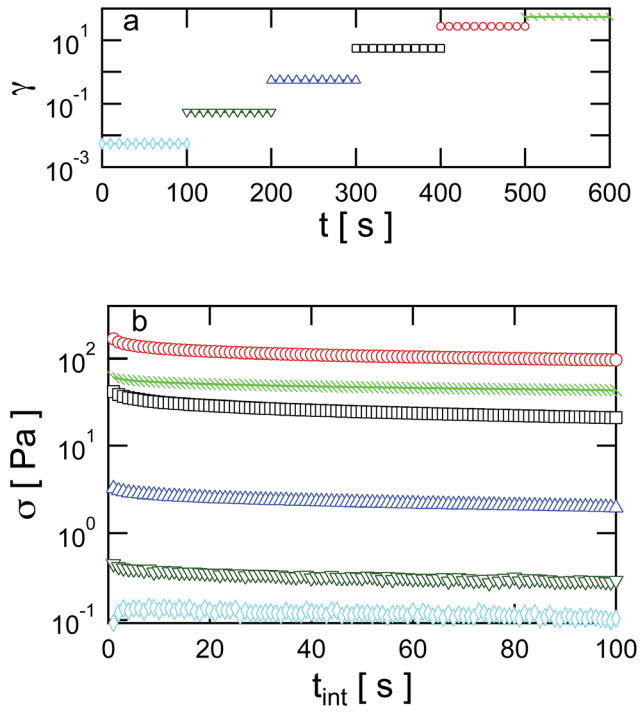

Fig. 3 (a) The strain schedule for the stress relaxation test for one representative e-gel – a single e-gel is held for 100 seconds at increasing strains of $\gamma = 0.0055$ (◇), 0.055 (▽), 0.55 (△), 5.5 (□), 27.5 (○), and 55 (\). (b) The stress response σ as a function of t_{int} shows an increasing stress with increasing strain until $\gamma = 55$ (\). Note the lack of complete stress relaxation during each interval.

strain is applied to the e-gel with a schedule shown in Fig. 3(a). This results in an increase in the measured stress held by the e-gel until a rotational strain $\gamma > 27.5$ (○), providing a range for the yield strain γ_y: $27.5 < \gamma_y < 55$ [Fig. 3(b)]. After yielding, the detachment of the gel from the rheological tools is observed using confocal-rheology. A yield strain for a biological or synthetic polymer network in this range is highly unexpected.[21,22] We also gather an estimate for the yield stress $\sigma_y > 100$ Pa that is two orders of magnitude larger than that of gelatin at a similar concentration.[23] Interestingly, the stress response of an e-gel exhibits a relaxation during each interval but does not decay completely. The non-zero value of stress as $t_{int} \rightarrow \infty$ is similar to the rheological response of a solid, which may signify inter-protein crosslinking in the e-gel.[19]

To elucidate the effect of large strain deformations on the e-gel we perform a strain recovery test; we are able to simultaneously evaluate the linear elastic modulus and quantify the e-gel's ability to recover from large strains [Fig. 4]. The test consists of the application of a strain at a rate of 0.25 s^{-1} up to a fixed maximum γ_{app}; we do not observe a systematic dependence on strain rate (data not shown). Once γ_{app} is reached, the rheometer is instructed to apply no torque on the e-gel, allowing the e-gel to relax to an equilibrium strain position γ_{eq} where $\sigma = 0$. The percentage of strain recovered $\Delta = 100\left(1 - \frac{\gamma_{eq}}{\gamma_{app}}\right)$ is recorded for each γ_{app} (closed symbols); the strain history of a representative e-gel can be seen in Fig. 4(a) with γ_{app} and γ_{eq} defined in the inset for the interval in the dashed box. At γ_{eq}, G' is measured at a strain amplitude of $\gamma = 10^{-2}$ and frequency $f = 1.0$ Hz and normalized by G_0, the shear modulus at $\gamma_{app} = 0$ (open symbols). This is repeated on the same sample with increasing γ_{app} for three different e-gels.

The results of the e-gel strain recovery can be separated into two regimes [Fig. 4(b)]. For $\gamma_{app} < 5$, the e-gel responds quasi-elastically with $\Delta > 70\%$ and $G'/G_0 \leq 1$. The slight modulus decrease could be an indicator of the stretching or kinking of structural components in the e-gel.[24] For $\gamma_{app} > 5$, the continual decrease in Δ indicates a trend towards more plastic deformations, yet these deformations are accompanied by an increase in G'/G_0. The correlated changes in G' and Δ suggest that the applied strain energy is transformed into structural transformations within the e-gel leading to a higher elastic modulus.

This behavior is very unusual when compared to other biopolymer gels. An elastic recovery of $\Delta \approx 70\%$ at $\gamma_{app} \approx 5$ is remarkable; a strain of only $\gamma_{app} = 1.0$ would cause yielding in a polymer gel like polyacrylamide and result in $\Delta = 0\%$.[22]

The significant plastic deformation at large γ_{app}, coupled with increasing G', is reminiscent of strain hardening found in crystalline solids.[25,26] This type of strain hardening has also

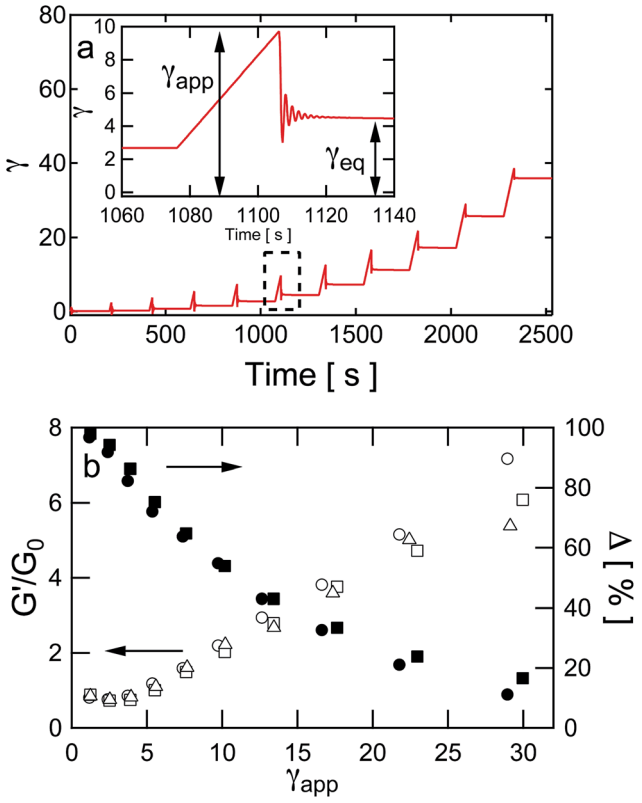

Fig. 4 (a) A representative strain history for an e-gel undergoing a strain recovery test. Each gel is subject to stepwise increasing applied rotational strains up to a maximum γ_{app} and allowed to relax back to an equilibrium position after each strain γ_{eq}; the inset highlights the interval in the dashed box. The new equilibrium strain position is recorded and a modulus measurement is made before the next strain cycle. (b) Percent strain recovery Δ (●, ■, and ▲) and G' (○, □, and Δ) as a function of γ_{app} for three e-gels reveal a strain hardening effect.

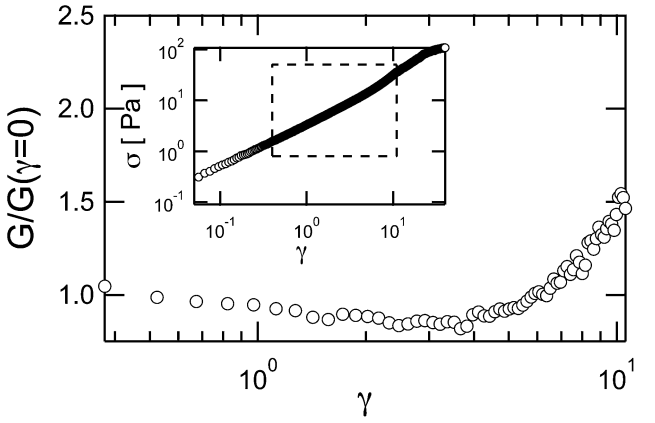

Fig. 5 A rotational strain ramp for one e-gel at $\dot{\gamma} = 0.1\ s^{-1}$ reveals a stress response (inset) that is initially elastic until a change in curvature highlighted by the dashed box. (main) The elastic modulus G is calculated from a 3-point numerical derivative after smoothing and thinning the data in the dashed box and normalized by the small strain elastic modulus $G(\gamma = 0)$.

been observed in *Nephila pilipes* dragline spider silk fibers.[27] In both cases, the plastic deformation decreases the crystallinity of the material. However, the e-gel is found to be a relatively disordered material, as discussed in Section 3, and it is unlikely that e-gel deformation further decreases the order in the system. We speculate that the observed strain hardening is likely a result of an increase in order in the e-gel network.

We observe a strain stiffening response of the e-gel as seen through a rotational strain ramp at a strain rate $\dot{\gamma} = 0.1\ s^{-1}$ [Fig. 5]. The stress response, shown in Fig. 5 (inset), reveals an initial elastic response followed by a nonlinear increase in stress in the region indicated by the dashed box. The slope of the boxed stress–strain data, after binning, is calculated with a numerical derivative to determine the elastic modulus G and is normalized by the small strain modulus $G(\gamma = 0)$. Strain stiffening occurs when $G/G(\gamma = 0) > 1$ near $\gamma = 6$; the elastic regime is consistent with Fig. 4.

Though the strain ramp reveals strain stiffening, a differential modulus measurement is performed to provide a more quantitative understanding [Fig. 6]. We superpose an oscillatory stress $\delta\sigma_f(t) \sim \mathrm{Re}[\delta\sigma e^{ift}]$ with a rotational prestress σ_0 at $f = 1.0$ Hz. We adhere to the restriction $|\delta\sigma| \leq \sigma_0/10$ and measure the differential elastic modulus $K'_f = \mathrm{Re}[\delta\sigma_f(t)/\delta\gamma_f(t)]$.[28] The normalized differential modulus K'/G_0 remains constant at small σ_0 and begins to increase when σ_0 approaches 10 Pa.

A critical prestress σ_{crit} is defined as $\sigma_{crit} = \sigma(K'/G_0 = 1.5)$ to mark the beginning of strain stiffening behavior. Normalizing each e-gel data by σ_{crit} collapses the four tests onto one curve. The solid line representing the power-law relation

$$K'/G_0 \sim (\sigma_0/\sigma_{crit})^{\kappa} \quad (2)$$

with $\kappa = 1$ is plotted to show that the local e-gel scaling behavior is $\kappa < 1$.

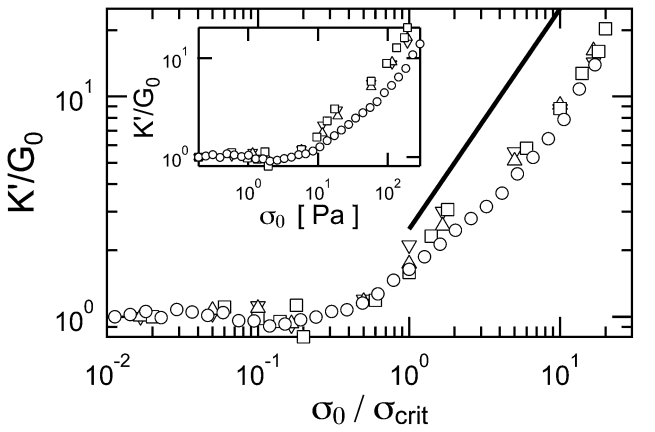

Fig. 6 (inset) The differential modulus K' normalized by G_0 as a function of rotational prestress σ_0 measured for four e-gels (○, □, △, ▽). (main) When normalized by $\sigma_{crit} = \sigma(K'/G_0 = 1.5)$, all data sets collapse onto one curve. When $\sigma_0/\sigma_{crit} < 1$ the response is elastic. And when $\sigma_0/\sigma_{crit} > 1$, the e-gel strain stiffens at a rate that is slower than the solid line: $K'/G_0 \sim (\sigma_0/\sigma_{crit})^{\kappa}$ where $\kappa = 1$.

5 Discussion

Characterization of e-gel strain stiffening provides a significant deviation from semi flexible biopolymer networks such as actin and fibrin. A polymer is fully extended when the end-to-end displacement length of the polymer R reaches the contour length, ℓ_c or $x = R/\ell_c = 1$. Considering the generic force-extension relation $f \sim 1/(1-x)^{\alpha}$ and $\partial f/\partial x \sim K$, we can derive the scaling of the differential modulus $K \sim \sigma^{(\alpha+1)/\alpha}$ where $\kappa = (\alpha+1)/\alpha$. The nonlinear force needed to extend most biopolymers to $x = 1$ diverges as $f \sim 1/(1-x)^2$, as defined by the Wormlike Chain WLC model.[29] Therefore, the WLC model $\alpha = 2$ yields a scaling of $\kappa \sim \frac{3}{2}$.[22,30,31] Although the nonlinear scaling of many biopolymers can be explained by this model, the strain stiffening we observe in the e-gel scaling is at a significantly lower power $\kappa < 1$. This model assumes a semi-flexible polymer, so the variation in κ values supports our initial approximation of the fibroin as a flexible polymer.

The force-extension relation for flexible freely jointed chains, $f \sim x(3-2x)/(1-x)$, diverges at a slower rate than the WLC.[32] This implies that e-gels should stiffen at a lower pace than semi-flexible biopolymers, consistent with our results. However, using the value for κ found in Fig. 6 of $0 < \kappa < 1$ requires $\alpha < 0$ and results in a polynomial stress–strain relationship that does not diverge as predicted for flexible polymers. The discrepancy of the nonlinear elasticity of silk e-gels compared to both flexible and semi-flexible polymers is likely a consequence of dynamic protein interactions. These polymer models ignore the ability of inter-protein bonds to break and reform during extension from shear, but we know that native silks undergo strain induced protein reorganization and association on multiple length scales.[33]

One such model describes that the extension of α-helices can cause unraveling and reorganizations into β-sheets.[34] Breaking of the helix structure increases ℓ_c, which would provide a smaller value for κ.[35] This would imply that the source of nonlinear elasticity found in silk e-gels comes from a combination of entropic costs through extensions combined with dynamic inter-protein interactions. A similar effect could be obtained through the unwinding of random coil structures into β-sheets.

In addition to increasing ℓ_c, the transition to β-sheets leads to a loss of recovered strain, consistent with the decrease in Δ in Fig. 4. Moreover, the shear induced β-sheet and crystallite formation would subsequently increase G'/G_0 as Δ decreases, providing the strain hardening effect. We speculate that beyond the strains required for β-sheet production, additional strain energy can provide a pathway for adjacent β-sheets to coalesce into nano-crystallites. These nano-crystallites are considered to be an essential component for enhancing the strength of the inherently amorphous structure within silk fibers.[36]

6 Conclusions

Our results clearly show that the electrogelation process transforms a mildly viscoelastic silk protein solution into a robust elastic network. One particularly interesting aspect of the electrogelation process is the apparent *in situ* assembly of protein into a gel that exhibits behavior similar to crosslinked networks without additional chemical moieties. Moreover, the ability of the e-gel to convert into a stronger material through the application of a large external shear stress provides a unique opportunity for engineering adaptive soft materials.

Our results indicate that the rheological response of silk e-gels cannot be simply explained using existing polymer physics models. The significant range of the linear viscoelastic regime and the dramatic yield strains far exceed nearly all biopolymers. These unique features all stem from electrolytically induced inter-protein assembly where protein interactions, *i.e.* material properties, are programmable through shear. Our results provide a starting point for *in situ* measurements of conformational changes through the application of shear, where we anticipate that gels of reconstituted silk may provide distinct insights into systems of self-associating proteins.

Acknowledgements

This work was supported by the Air Force Office of Scientific Research through grants no. FA9550-07-1-0130, FA9550-14-1-0171 and FA9550-14-1-0015. APT would also like to thank the Walter G. Mayer Endowed Scholarship Fund for the support. The authors appreciate Jeffrey Urbach for his helpful discussions and Peter Olmsted for insightful manuscript feedback.

References

1 D. N. Rockwood, R. C. Preda, T. Yucel, X. Wang, M. L. Lovett and D. L. Kaplan, *Nat. Protoc.*, 2011, **6**, 1612–1631.
2 G. G. Leisk, T. J. Lo, T. Yucel, Q. Lu and D. L. Kaplan, *Adv. Mater.*, 2010, **22**, 711–715.
3 T. Yucel, N. Kojic, G. G. Leisk, T. J. Lo and D. L. Kaplan, *J. Struct. Biol.*, 2010, **170**, 406–412.
4 C. Vepari and D. L. Kaplan, *Prog. Polym. Sci.*, 2007, **32**, 991–1007.
5 G. H. Altman, F. Diaz, C. Jakuba, T. Calabro, R. L. Horan, J. Chen, H. Lu, J. Richmond and D. L. Kaplan, *Biomaterials*, 2003, **24**, 401–416.
6 M. Boulet-Audet, F. Vollrath and C. Holland, *Phys. Chem. Chem. Phys.*, 2011, **13**, 3979–3984.
7 S. Rammensee, D. Huemmerich, K. D. Hermanson, T. Scheibel and A. R. Bausch, *Appl. Phys. A: Mater. Sci. Process.*, 2005, **82**, 261–264.
8 C. Mo, C. Holland, D. Porter, Z. Shao and F. Vollrath, *Biomacromolecules*, 2009, **10**, 2724–2728.
9 Q. Lu, Y. Huang, M. Li, B. Zuo, S. Lu, J. Wang, H. Zhu and D. L. Kaplan, *Acta Biomater.*, 2011, **7**, 2394–2400.
10 S. Sofia, M. B. McCarthy, G. Gronowicz and D. L. Kaplan, *J. Biomed. Mater. Res.*, 2000, **54**, 139–148.
11 Y. Lin, X. Xia, K. Shang, R. Elia, W. Huang, P. Cebe, G. Leisk, F. Omenetto and D. L. Kaplan, *Biomacromolecules*, 2013, **14**, 2629–2635.
12 N. Kojic, M. J. Panzer, G. G. Leisk, W. K. Raja, M. Kojic and D. L. Kaplan, *Soft Matter*, 2012, **8**, 6897–6905.

13 C.-Z. Zhou, F. Confalonieri, M. Jacquet, R. Perasso, Z.-G. Li and J. Janin, *Proteins: Struct., Funct., Genet.*, 2001, **44**, 119–122.
14 D. Wilson, R. Valluzzi and D. Kaplan, *Biophys. J.*, 2000, **78**, 2690–2701.
15 H. Shulha, C. P. Foo, D. L. Kaplan and V. V. Tsukruk, *Polymer*, 2006, **47**, 5821–5830.
16 H.-J. Jin and D. L. Kaplan, *Nature*, 2003, **424**, 1057–1061.
17 M. M. Castellanos, J. A. Pathak and R. H. Colby, *Soft Matter*, 2014, 122–131.
18 P. Sollich, F. Lequeux, P. Hébraud and M. Cates, *Phys. Rev. Lett.*, 1997, **78**, 2020–2023.
19 D. T. N. Chen, Q. Wen, P. A. Janmey, J. C. Crocker and A. G. Yodh, *Annu. Rev. Condens. Matter Phys.*, 2010, **1**, 301–322.
20 W. Zhang, Q. Xu, S. Zou, H. Li, W. Xu, X. Zhang, Z. Shao, M. Kudera and H. E. Gaub, *Langmuir*, 2000, **16**, 4305–4308.
21 K. A. Erk, K. J. Henderson and K. R. Shull, *Biomacromolecules*, 2010, **11**, 1358–1363.
22 C. Storm, J. J. Pastore, F. C. MacKintosh, T. C. Lubensky and P. A. Janmey, *Nature*, 2005, **435**, 191–194.
23 J. N. Wilking and T. G. Mason, *Phys. Rev. E: Stat., Nonlinear, Soft Matter Phys.*, 2008, **77**, 055101.
24 S. Münster, L. M. Jawerth, B. A. Leslie, J. I. Weitz, B. Fabry and D. A. Weitz, *Proc. Natl. Acad. Sci. U. S. A.*, 2013, **110**, 12197–12202.
25 G. I. Taylor, *Proc. R. Soc.*, 1934, 1–18.
26 Z. S. Basinski, *Philos. Mag.*, 1964, **9**, 51–80.
27 N. Du, Z. Yang, X. Y. Liu, Y. Li and H. Y. Xu, *Adv. Funct. Mater.*, 2010, **21**, 772–778.
28 M. Gardel, F. Nakamura, J. Hartwig, J. Crocker, T. Stossel and D. Weitz, *Phys. Rev. Lett.*, 2006, **96**, 088102.
29 J. F. Marko and E. D. Siggia, *Macromolecules*, 1995, **28**, 8759–8770.
30 Y.-C. Lin, N. Y. Yao, C. P. Broedersz, H. Herrmann, F. C. MacKintosh and D. A. Weitz, *Phys. Rev. Lett.*, 2010, **104**, 058101.
31 M. L. Gardel, J. H. Shin, F. C. MacKintosh, L. Mahadevan, P. Matsudaira and D. A. Weitz, *Science*, 2004, **304**, 1301–1305.
32 E. Evans and K. Ritchie, *Biophys. J.*, 1999, **76**, 2439–2447.
33 C. Holland, A. E. Terry, D. Porter and F. Vollrath, *Polymer*, 2007, **48**, 3388–3392.
34 Z. Qin and M. J. Buehler, *Phys. Rev. Lett.*, 2010, **104**, 198304.
35 S. Keten and M. Buehler, *Phys. Rev. E: Stat., Nonlinear, Soft Matter Phys.*, 2008, **78**, 061913.
36 S. Keten, Z. Xu, B. Ihle and M. J. Buehler, *Nat. Mater.*, 2010, **9**, 359–367.